CryoEM reveals unprecedented binding site for $Na_V1.7$ inhibitors enabling rational design of potent hybrid inhibitors

Marc Kschonsak[1*], Christine C. Jao[1*], Christopher P. Arthur[1], Alexis L. Rohou[1], Philippe Bergeron[2], Daniel Ortwine[2], Steven J. McKerrall[2], David H. Hackos[3], Lunbin Deng[3], Jun Chen[4], Peter S. Dragovich[2], Matthew Volgraf[2], Matthew R. Wright[5], Jian Payandeh[1,#], Claudio Ciferri[1,#], John C. Tellis[2,#]

[1]Genentech Inc., Structural Biology; South San Francisco, CA, United States.
[2]Genentech Inc., Discovery Chemistry; South San Francisco, CA, United States.
[3]Genentech Inc., Neuroscience; South San Francisco, CA, United States.
[4]Genentech Inc., Biochemical and Cellular Pharmacology; South San Francisco, CA, United States.
[5]Genentech Inc., Drug Metabolism and Pharmacokinetics; South San Francisco, CA, United States.

[#]Corresponding authors. Email: jpayandeh@exelixis.com (J.P); ciferri.claudio@gene.com (C.C.); tellis.john@gene.com (J.C.T.).

Author Contributions: J.P., C.C., and J.C.T. designed research, M.K., C.J., C.P.A., A.R., D.H., and J.C., performed research, J.C.T, P.B., D.O., S.M., P.S.D., and M.V. analyzed data and contributed to compound design. J.C.T., C.C., J.P., and M.K. wrote the paper.

Competing Interest Statement: The authors declare no competing financial interest

Abstract

The voltage-gated sodium (Na_V) channel $Na_V1.7$ has been identified as a potential novel pain target due to its striking human genetics. However, clinically available drugs (e.g. lidocaine, carbamazepine, etc.) are not selective among the nine Na_V channel subtypes, $Na_V1.1$-$Na_V1.9$, and the two currently known classes of $Na_V1.7$ subtype-selective inhibitors (aryl- and acylsulfonamides) have undesirable characteristics that may limit their development. Moreover, understanding of the structure-activity relationships of the acylsulfonamide class of $Na_V1.7$ inhibitors, exemplified by the clinical development candidate **GDC-0310**, has been based solely on a single co-crystal structure of an arylsulfonamide inhibitor series. To advance inhibitor design targeting the $Na_V1.7$ channel, we established an iterative system to routinely obtain high-resolution ligand-bound $Na_V1.7$ structures using cryogenic electron microscopy (cryo-EM). We report that **GDC-0310** engages the $Na_V1.7$ voltage-sensing domain 4 (VSD4) through an unexpected binding mode orthogonal to the arylsulfonamide class binding pose, which identifies a previously unknown ligand binding site in Na_V channels. This finding enabled the design of a novel hybrid inhibitor series that bridges the aryl and acylsulfonamide binding pockets and allows for the generation of molecules with substantially differentiated structures and properties. Overall, this study highlights the power of cryo-EM methods to pursue challenging drug targets using iterative and high-resolution structure-guided inhibitor design. It also underscores an important role of the membrane bilayer in the discovery of selective Na_V channel modulators.

Introduction

Voltage-gated sodium (Na_V) channels initiate and propagate action potentials in excitable tissues and play important roles in health and disease.[1,2] The $Na_V1.7$ channel is expressed predominantly in the peripheral nervous system and genetic studies have identified compelling loss-of-function and gain-of-function phenotypes in human pain syndromes, prompting significant efforts to develop $Na_V1.7$-selective inhibitors as potential novel analgesic drugs.[3-5] Na_V channels contain 24-transmembrane segments linked in four homologous domains (DI-DIV), where four peripheral voltage-sensor domains (VSD1-4) surround a central ion-conducting pore module that houses the ion selectivity filter and key ligand and toxin receptor sites. Traditionally, all clinically available Na_V channel inhibitors lack significant molecular selectivity among the $Na_V1.1$–1.9 subtypes owing to the high sequence conservation found at the ligand binding site within the central cavity of the ion conducting pore module.[5,6]

A breakthrough study in 2013 by McCormack and colleagues reported the discovery of an arylsulfonamide antagonist, **PF-04856264**, that bound to an unprecedented receptor site in VSD4 with demonstrated molecular selectivity for human $Na_V1.7$ over other subtypes.[7] However, the related development candidate **PF-05089771** did not meet clinical endpoints in human subjects with painful diabetic peripheral neuropathy, possibly due to poor target coverage and the intolerable doses required to achieve efficacy.[8-10] Additionally, an alternate acylsulfonamide inhibitor that also targeted the VSD4 receptor

site in $Na_V1.7$, **GDC-0276**, was halted in Phase I clinical trials due to safety concerns and potential off-target effects likely attributed to the high lipophilicity of the compound.[11,12] To date, selective $Na_V1.7$ inhibitors with an improved therapeutic index relative to these clinical-stage compounds have not yet been identified, and this absence underscores the need to optimize such molecules using modern, structure-guided design approaches.

The inherent complexity and dynamic nature of human Na_V channels have historically presented significant barriers to obtaining high-resolution experimental structural information, especially of inhibitor-bound complexes.[13] Using an engineered human VSD4 $Na_V1.7$-Na_VAb bacterial channel chimera and X-ray crystallography, the binding mode of the **GX-936** arylsulfonamide inhibitor (Supplementary Figure 1) revealed that the anionic sulfonamide group engages the fourth arginine gating charge (R4) to trap VSD4 in an activated conformation, which stabilizes a non-conductive, inactivated state of the channel.[14] While determinants of subtype selectivity and structure-activity relationships (SAR) of the arylsulfonamide inhibitor class could be rationalized by the **GX-936** co-crystal structure, additional ligand-bound structures of suitable resolution were not returned by the $Na_V1.7$-Na_VAb chimeric channel crystallography system. This shortcoming led molecular docking studies to presume that the acylsulfonamide inhibitors also bound VSD4 in an analogous manner, despite points of inexplicable SAR.[15] The overall paucity of direct structural information has made the optimization of $Na_V1.7$ inhibitors challenging, with many questions about the determinants of potency, selectivity, and the relationship between the acylsulfonamide and arylsulfonamide inhibitor classes remaining unanswered.

Over the last three decades, protein crystallography and structure-based drug design (SBDD) have become gold standards across the pharmaceutical industry for the identification of ligand binding pockets and the optimization of drug candidates for clinical development. While SBDD has proven successful for many important targets, including G protein-coupled receptors (GPCRs),[16] its applicability to several membrane protein targets, such as Na_V channels, has been limited due to the extreme difficulties with their iterative crystallization and structure determination.[13] Cryogenic electron microscopy (cryo-EM) has recently emerged as a transformative technique to determine the high-resolution structures of diverse protein targets and has proven particularly effective for membrane proteins that are recalcitrant to crystallization.[17] Despite this breakthrough, cryo-EM structure determination of membrane targets in complex with small or large molecule therapeutics frequently remains retrospective and is often enabled after the advancement of key molecules into the clinic.[18,19] Sluggish turn-around times and modest resolutions typically afforded by cryo-EM have limited its application for real-time SBDD efforts. Here, we describe a system for the iterative determination of high-resolution $Na_V1.7$ small molecule co-structures via cryo-EM that has led to the development of a novel class of inhibitors. Critical to this advancement has been establishment of a robust protocol for sample preparation and structure determination and the enablement of the first structure of an acylsulfonamide bound to $Na_V1.7$ VSD4, revealing a previously unknown pocket between the S3 and S4 helices. Consequently, a novel hybrid inhibitor series bridging the aryl and acylsulfonamide pockets was generated. Our work exemplifies the deployment of cryo-EM as a workhorse structural biology tool in an active medicinal

121 chemistry campaign and thus represents an important milestone toward Na_V channel drug
122 discovery.
123
124
125 **Results**
126
127 **Structure of the G-3565-VSD4 Na_V1.7-Na_VPas channel complex in lipid nanodiscs**
128 Our approach to establish an iterative, high-resolution system to enable Na_V1.7
129 SBDD was ultimately guided by three observations: our repeated failure to generate well-
130 diffracting crystals of the Na_V1.7-Na_VAb bacterial channel chimera system,[14] our difficulty
131 of reproducibly expressing a suitable amount of full-length human Na_V1.7 channel,[20,21] and
132 the very limited local resolution observed at VSD4 in all available human Nav1.7 cryo-EM
133 structures.[22,23] Thus, we sought to exploit an engineered human VSD4-Na_V1.7-Na_VPas
134 cockroach channel chimeric construct that had been previously shown to complex with
135 small molecule inhibitors and peptide toxins known to target VSD4.[21] The robust protein
136 yields following expression and purification allowed us to readily pursue reconstitution of
137 the VSD4-Na_V1.7-Na_VPas channel into lipid nanodisc with high recovery (Supplementary
138 Figure 2). Small molecule inhibitors were added prior to sample vitrification, followed by
139 cryo-EM data collection and processing procedures, which allowed us to routinely obtain
140 3D-reconstructions in the 2.2-3.0 Å resolution range (Figure 1, Supplementary Figure 3).
141
142 The VSD4-Na_V1.7-Na_VPas chimera displays the expected domain-swapped
143 arrangement with numerous densities assigned as phospholipids bound to the channel,
144 confirming the maintenance of a native membrane-like environment (Figure 1). As seen in
145 previous Na_VPas structures,[21,24,25] the ion-conducting pore module of the VSD4-Na_V1.7-
146 Na_VPas chimeric channel is closed, consistent with a nonconductive or inactivated state.
147 The quality and resolution of our structure allowed us to assign 112 water molecules for
148 the highest resolution structure (Figure 1, Video 1). The visualization of many well-
149 resolved water molecules bound within the VSDs and coordinated within the ion selectivity
150 filter provides new insights into the interactions that might occur during gating charge
151 transfer and ion conduction, respectively.
152
153 Although we were able to determine the crystal structure of VSD4-Na_VAb bound
154 to the arylsulfonamide inhibitor **GX-936**,[14] no well-diffracting crystals were obtained for
155 any other arylsulfonamide compounds despite years of continued effort. Arylsulfonamide
156 **GNE-3565** is representative of an advanced series of arylsulfonamide class Na_V1.7
157 inhibitors that demonstrates channel blockage at subnanomolar concentrations with mixed
158 subtype selectivity (Figure 2A). We complexed **GNE-3565** with the VSD4 Na_V1.7-Na_VPas
159 channel-nanodisc system and employed cryo-EM to assess its overall binding pose (Figure
160 2B, C). The 2.9 Å resolution cryo-EM map revealed that the S1-S2 and S3-S4 helices from
161 VSD4 form a clamshell-like structure that closes over **GNE-3565** (Figure 2D, E,
162 Supplementary Data Figure 4A-D, Supplementary Data Table 1), similar to the binding
163 pose reported for **GX-936**.[14] Specifically, the ionized arylsulfonamide group of **GNE-**
164 **3565** (measured pKa = 5.8) bisects VSD4 to salt-bridge directly to R4 on the S4 helix,
165 while the central phenyl ring extends perpendicular between the S2 and S3 helices to
166 directly contact established subtype-selectivity determinants Tyr1537 and Trp1538 on the

S2 helix (Figure 2A-D). As for **GX-936**, the **GNE-3565** arylsulfonamide VSD4 receptor binding site can be divided into three regions: an anion-binding pocket, a selectivity pocket, and a lipid-exposed pocket (Figure 2D). The root-mean-square deviation (RMSD) between the **GNE-3565**-VSD4 and the **GX-936**-VSD4 structures[14] is 0.667 (714 to 714 atoms), (Supplementary Figure 5A), supporting long-held assumptions by medicinal chemistry teams that all structurally-related arylsulfonamides should be expected to complex to VSD4 through similar determinants.[8,26-31]

Structure of the acylsulfonamide GDC-0310 in complex with the VSD4 $Na_V1.7$-Na_VPas channel

To investigate the binding pose of a representative $Na_V1.7$ selective acylsulfonamide, **GDC-0310** (Figure 3A) was complexed with the VSD4 $Na_V1.7$-Na_VPas channel in nanodiscs and a cryo-EM structure was determined to 2.5 Å resolution (Figure 3B-D, Supplementary Data Figure 3G-J, Supplementary Data Table 1). Remarkably, the binding mode of **GDC-0310** revealed an unexpected and previously unknown pocket that formed between the S3 and S4 helices (Figure 3B-E). While the aryl and acyl moieties of **GDC-0310** and **GNE-3565** bind in the same region, the remainder of the acyl receptor site is orthogonal to the corresponding binding domain reported for the aryl class (Figure 3B-D). In detail, the anionic acylsulfonamide of **GDC-0310** participates in salt-bridge bonding interactions with R4 and R3 through the carbonyl and sulfonamide oxygen atoms, respectively (Figure 3F). Moreover, the aryl ring of the **GDC-0310** splits the S3 and S4 helices to occupy a lipophilic pocket, displacing the S3 helix laterally by ~3 Å relative to the **GNE-3565**-VSD4 structure (Figure 3G). Our cryo-EM inhibitor bound structures serve to highlight a dynamic environment in VSD4 where the S1-S4 helixes can be differentially separated by distinct small molecule binding poses (Figure 2D, Figure 3D).

It is notable that the cyclopropyl substituent of **GDC-0310** makes effective van der Waals interactions with I1574 and I1588 from S3 and I1601 and I1604 on S4 (Figure 3G), while the alpha-methylbenzylamine "tail" region sits almost entirely within the lipid bilayer (Figure 3A, C), where density for this portion of the inhibitor is only poorly resolved (Figure 3E). Considering the relative depth of the **GDC-0310** binding site in relation to the membrane-water interface (~8 Å), our structure suggest a membrane access pathway for acylsulfonamides to the VSD4 receptor site, which has important implications for understanding the pharmacology, SAR, and potential development liabilities of the series.[32] Notably, this structure also reveals that the Tyr1537 side-chain on S2 exists in a down rotamer and does not contact **GDC-0310** directly, which provides the first direct structural rationale for why the selectivity profiles between the acyl and arylsulfonamide classes differ substantially (Figure 3D, *vide infra*).[33]

Structure-based rational design of hybrid $Na_V1.7$ inhibitors

Upon inspection of the superimposed **GNE-3565**-aryl and **GDC-0310**-acyl structures, we could immediately envision a novel class of hybrid inhibitors that would simultaneously occupy both the aryl- and acylsulfonamide binding pockets (Figure 4A, B). Such an enlarged hybrid binding pocket would offer unique opportunities to gain potency directly from ligand-protein interactions, which might enable removal of the hydrophobic lipid-facing tail groups seen in all previous generations of VSD4-targeting Na_V channel

213 inhibitors. These groups have typically been critical for maintaining potency, but use of
214 the plasma membrane to drive membrane-bound target occupancy is largely nonspecific,
215 and potentially introduces off-target liabilities that can contribute to toxicity. However, it
216 was unclear if this hybrid conformation of the VSD4 domain could accommodate the
217 described inhibitors and/or whether it was accessible during any stage of $Na_V1.7$ channel
218 activation. We therefore set out to demonstrate proof-of-concept that appropriately
219 designed small molecules could induce this hypothesized receptor state while inhibiting
220 channel function with meaningful potency.
221
222 **GDC-0310** was a relatively unattractive starting point for hybridization because of
223 its high molecular weight (543 g/mol) and lipophilicity (cLogP = 5.2). Accordingly,
224 analysis of historical data identified progenitor compound **1**, which offers reasonable
225 potency against $Na_V1.7$ (IC_{50} = 25 nM, n = 8; Fig 4C) and reduced molecular weight (350
226 g/mol) and lipophilicity (cLogP = 2.7). Seeking to leverage existing knowledge of the
227 arylsulfonamide binding pocket, molecule **2** was synthesized in an attempt to directly graft
228 on a significant portion of the **GNE-3565** scaffold. Gratifyingly, this molecule retained
229 substantial potency, affording channel blockade at an IC_{50} of 47 nM (n = 8).
230
231 A cryo-EM structure of **2** bound to the VSD4 $Na_V1.7$-Na_VPas channel confirmed
232 that the molecule adopts the desired hybrid binding mode (Figure 4D). Here, the anionic
233 group of the novel hybrid compound binds in the same position as in the aryl and acyl
234 poses, interacting closely with R4, as seen for the aryl-like binding (Figure 4E). The aryl-
235 and acylsulfonamide-derived structural motifs of **2** occupy their expected positions in the
236 pockets formed between S2/S3 and S3/S4, respectively. Notably, in this hybrid
237 configuration, Y1537 adopts a similar arrangement as observed for the arylsulfonamides
238 (Figure 4F).
239
240 Encouraged by this result, we hoped to draw on previously established knowledge
241 of acylsulfonamide SAR to improve the potency of this compound. Established SAR within
242 the acylsulfonamide series suggested that replacement of the chloro substituent on the
243 benzamide fragment of the molecule with a cyclopropane would typically improve
244 potency. This SAR proved translatable to the hybrid class molecules, resulting in inhibitor
245 **3** (IC_{50} = 16 nM, n = 12; Figure 4C).
246
247 Further analysis of the cryo-EM structure of **2** revealed that the aryl ring in the
248 S2/S3 binding pocket was shifted ~1 Å away from the VSD4 core when compared to
249 arylsulfonamides such as **GNE-3565** (data not shown). The aryl ring in the S3/S4 pocket
250 exhibited better overlap with the analogous substituents in the **GDC-0310** structure. We
251 hypothesized that the acylsulfonamide moiety of **2**, which places the two aryl substituents
252 4.7 Å apart, might not be fully optimized for use in hybrid inhibitors. In comparison, an
253 arylsulfonamide moiety would position these two groups at a distance of ~3.3 Å. On this
254 basis we designed *N*-benzothiazolyl sulfonamide **4**, which demonstrated potent $Na_V1.7$
255 inhibition (IC_{50} = 9 nM, n = 8, Figure 4C).
256
257 Our last hypothesis was again validated with a cryo-EM co-structure of **4** bound to
258 the VSD4 $Na_V1.7$-Na_VPas channel (Figure 4G). Here, we observed the typical face-on pi-

stacking orientation of the S2/S3 substituent with Y1537 while maintaining efficient space filling in the S3/S4 pocket. Moreover, the efficient occupation of the non-membrane exposed regions of the binding pocket permitted the removal of the lipophilic tail of the molecule in **5**, where a CF_3 group replaces the cyclopentylmethyl substituent. Although this molecule shows reduced potency (IC_{50} = 74 nM, n = 8), lack of substantial small molecule contact with the lipid bilayer is an uncommon feature in all other known $Na_V1.7$ VSD4 domain inhibitors. These molecules serve as a key proof of concept, highlighting the power of cryoEM to yield new structural insights that can inspire the design of novel, structurally differentiated small molecule inhibitors.

Discussion

Iterative structure-based design is among the most powerful techniques to facilitate the development of small molecule drug candidates. Although a variety of technologies are capable of providing information about small molecule ligand-protein interactions, SBDD has traditionally been synonymous with the use of X-ray crystallography, with other techniques failing to rival its high resolution and fast cycle times. Here, we have demonstrated that a robust cryo-EM structure pipeline is sufficient to quickly provide co-structures at resolutions suitable for use in an active medicinal chemistry optimization campaign. Moreover, we have highlighted the power of structural methods, and cryo-EM in particular, to provide new and important insights into inhibitor design through the discovery of a previously unknown binding mode for acylsulfonamide $Na_V1.7$ inhibitors. We further note that our use of an engineered VSD4-$Na_V1.7$-Na_VPas chimeric channel construct was essential to produce high yields of recombinant protein capable of routinely returning multiple cryo-EM samples per preparation. This system repeatedly delivered high-resolution depictions of the VSD4 inhibitor binding site and thus strongly contrasts with all prior accounts of cryo-EM structures of full-length human $Na_V1.7$ channels.[22,23] Importantly, high quality cryo-EM maps at VSD4 in complex with ICA121431 have recently been reported from full-length human $Na_V1.3$ channel protein,[37] indicating that SBDD efforts targeting a particular Na_V channel subtype would benefit from exploring both engineered and native channel sample options at early project stages.

The co-structure of **GDC-0310** was critical to contextualize historical differences between aryl- and acylsulfonamide $Na_V1.7$ inhibitors, which include divergent SAR in the linker phenyl ring and tail regions, disparate Na_V family selectivity patterns, and differences in on-rates and off-rates.[12,15,33-36] Previous efforts to model acylsulfonamide binding have attempted to dock molecules into the **GX-936** co-structure and have proposed subtle changes in molecular register and/or pose to explain the non-translatable SAR.[15,38] Here, we demonstrate that the molecular features of aryl- and acylsulfonamide inhibitors diverge because they occupy distinct, but overlapping, pockets within the VSD4 domain.

The selectivity determinants of arylsulfonamide $Na_V1.7$ inhibitors have been well studied. Mutation of key non-conserved residues proximal to the binding pocket observed in the **GX-936** co-structure have been shown to alter $Na_V1.7$ potency consistent with selectivity patterns observed for other Na_V family members.[14] Typically, arylsulfonamides

305 have shown high levels of selectivity against $Na_V1.5$, $Na_V1.1$, and $Na_V1.4$, but lower
306 selectivity against $Na_V1.2$ and $Na_V1.6$. In comparison, several acylsulfonamides have been
307 characterized with very high selectivity over $Na_V1.2$ and $Na_V1.6$.[33] Interestingly, residues
308 forming the contours of the acylsulfonamide binding pocket show high sequence homology
309 across Na_V isoforms, suggesting that selectivity for this class is likely an allosteric
310 phenomenon. Nonetheless, the disparate binding pockets for these two inhibitor classes
311 provide a clear rationale for their historically divergent patterns of selectivity.
312
313 Our structure of **GDC-0310** provides a structural rationale for the relative slow
314 dissociation kinetics of acylsulfonamide inhibitors compared to arylsulfonamides.[33]
315 Specifically, the acylsulfonamide pocket is buried more deeply into the plasma membrane
316 than the arylsulfonamide pocket, and may be available only through a membrane-access
317 pathway that first involves partitioning of the molecule into the intramembrane space. In
318 comparison, the arylsulfonamide pocket is open to the outer membrane interface, offering
319 access from the solvent compartment. Slow dissociation kinetics are known to be
320 associated with membrane-access pathways for small molecules binding to transmembrane
321 proteins.[32,39] For example, the long duration of action of salmeterol (a long-acting β_2
322 adrenergic receptor agonist) is proposed to be a result of its membrane partitioning
323 properties. In comparison, salbutamol, which binds to the same target and site but through
324 a solvent-access pathway, shows much faster dissociation from the receptor.[40-46]
325
326 In addition to offering valuable information for retrospective analysis of historical
327 $Na_V1.7$ VSD4 domain inhibitors, the structure of **GDC-0310** inspired the development of
328 a class of structurally differentiated molecules that bind to a novel conformation of the
329 receptor. These hybrid molecules bridge both the S2/S3 and S3/S4 helical gaps, with the
330 anionic moiety situated centrally, interacting with the arginine network at the core of the
331 domain. We have demonstrated proof-of-concept that potent hybrid inhibitors can be
332 designed with fewer membrane-associated elements than prior generation $Na_V1.7$
333 inhibitors, and anticipate that this will offer opportunities to develop molecules with
334 improved lipophilic ligand efficiency and/or differentiated pharmacokinetic profiles.
335 Hybrid inhibitors can also access selectivity determinants from both the S2/S3 and S3/S4
336 pockets simultaneously, offering a tantalizing opportunity to develop exquisite selectivity
337 over other Na_V isoforms.
338
339 Beyond the scope of Na_V channel inhibitors, our experiences may also offer lessons
340 translatable to small molecule modulators of other transmembrane proteins. Specifically,
341 it is noteworthy to observe that both aryl- and acylsulfonamide inhibitors have access to
342 cryptic pockets that are not observable in the co-structures of the parent proteins. Designing
343 small molecules to "push" on a structural protein element is a common strategy in
344 medicinal chemistry, but it is often challenging to predict when such efforts will afford
345 new, well-defined binding pockets. As such, these designs are often met with failure and
346 quickly abandoned. However, some scenarios exist in which a cryptic pocket is more likely
347 to be found. In these cases, medicinal chemists are more often emboldened to continue
348 experimenting with designs that push into new areas of a protein binding pocket, even
349 when met with initial failure. For example, type II kinase inhibitors can be rationally
350 designed starting from a type I inhibitor structure by appending groups that push through

351 the DFG into the cryptic back pocket.[47] This pocket is not visible from the type I inhibitor
352 structure, but knowledge of the protein dynamics associated with the DFG-in/DFG-out
353 transition provides a rationale for exploring these designs. We speculate that
354 transmembrane intrahelical domains, particularly those in ion channels, transporters, and
355 GPCRs, may present similarly privileged protein structural motifs that are rich with
356 opportunities for the discovery of druggable cryptic pockets.
357
358 In summary, we have developed a robust pipeline for high-resolution structural
359 determination of small-molecule bound $Na_V1.7$ channels suitable for use in iterative
360 structure-based drug design campaigns. We also report the first co-structure of an
361 acylsulfonamide inhibitor bound to the VSD4 domain of $Na_V1.7$, revealing an unexpected
362 and unique binding mode. This finding provides clear rationale for previously
363 unexplainable divergence in the in vitro pharmacological behavior between the two
364 inhibitor classes, and inspired the development of hybrid inhibitors that merge structural
365 features from both inhibitor classes, engaging the receptor in a novel conformation. Our
366 findings highlight the power of cryoEM as an enabling drug discovery technology and offer
367 interesting learnings regarding ion channel structural dynamics that are potentially
368 applicable to other related targets and target classes.
369
370 **Materials and Methods**
371
372 **Generation of** VSD4-$Na_V1.7$-Na_VPas channel constructs
373 VSD4-$Na_V1.7$-Na_VPas chimeric constructs were used as described previously.[21] In brief,
374 optimized coding DNA for $Na_V1.7$ VSD4-Na_VPaS chimeras with N-terminal tandem
375 StrepII and FLAG tag was cloned into a pRK vector with CMV promoter. HEK293 cells
376 in suspension were cultured in SMM 293T-I medium under 5% CO_2 at 37°C and
377 transfected using PEI when the cell density reached 4×10^6 cells per ml. Transfected cells
378 were harvested 48 hours after transfection. The Dc1a toxin coding DNA from *Diguetia*
379 *canities* was cloned into a modified pAcGP67A vector downstream of the polyhedron
380 promoter and an N-terminal 6x HIS tag. Recombinant baculovirus was generated using the
381 Baculogold system (BD Biosciences) and *Trichoplusia ni* cells were infected for protein
382 production. The supernatant was harvested 48 h post-infection.
383
384 **Protein expression and purification:**
385 One hundred fifty grams of cell pellet was resuspended in 500mL of 25mM Hepes pH 7.5,
386 200mM NaCl, 1ug/mL benzonase, 1mM PMSF, and Roche protease inhibitor tablets. Cells
387 were lysed by dounce homogenization. Proteins were solubilized by addition of 2% GDN
388 (Avanti) with 0.3% cholesteryl hemisuccinate (Avanti) for 2 hours at 4ºC. Cell debris was
389 separated by ultracentrifugation at 40,000 rpm at 4ºC. Affinity purification using anti-Flag
390 resin was performed by batch binding for 1 hour at 4ºC. The resin was washed with 5CV
391 Purification Buffer (25mM Hepes pH 7.5, 200mM NaCl, 0.01% GDN). Another 5CV
392 wash was performed using Purification Buffer supplemented with 5mM ATP and 10mM
393 $MgCl_2$. Proteins were eluted in 6 CV Purification Buffer with 300ug/mL Flag peptide.
394 Proteins were subjected to another round of affinity purification using StrepTactin resin
395 (IBA). Proteins were eluted, and concentrated to ~ 5 mg/mL. For the compound **2**
396 containing sample, instead of nanodisc reconstitution VSD4-$Na_V1.7$-Na_VPas was

397 incubated overnight with Dc1a toxin at a 2:1 molar ration of toxin:VSD4-Na_V1.7-Na_VPas.
398 The eluted sample was concentrated to 100uL, and separated on Superose 6 3.2/300.
399
400 For nanodisc reconstitution used for the samples containing **GNE-3565, GDC-0310** and
401 compound **4**, a 200-molar excess of lipid mix (3POPC:1POPE:1POPG resuspended in
402 50mM Hepes pH7.5, 100mM NaCl, 5mM $MgCl_2$, 1% CHAPS) was added to detergent-
403 solubilized protein and incubated on ice for 30 minutes. A four-molar excess of scaffold
404 protein (MSP1E3D1, Sigma) was added to the protein-lipid mix, and incubated on ice for
405 another 30 minutes. To remove detergent, BioBeads (Bio-Rad) were added to 0.25 mg/mL,
406 and incubated overnight at 4ºC. To remove the empty nanodiscs, the sample was subjected
407 to a round of affinity purification using Strep-Tactin (IBA). The eluted sample was
408 concentrated to 100uL, and separated on Superose 6 3.2/300. Peak fractions were
409 combined, and split into four samples. Fifty uM of the small molecule of interest was
410 added to each sample, and incubated at 22ºC for 10 minutes. The nanodisc reconstituted
411 samples were crosslinked with 0.05% glutaraldehyde (Electron Microscopy Sciences) then
412 quenched with 1M Tris pH 7.0. Samples at 2 mg/mL were used for grid freezing.
413
414
415 **CryoEM sample preparation and data acquisition**
416 CryoEM grids for the small molecule VSD4-Na_V1.7-Na_VPas chimeric complexes shown
417 in this study were prepared as follows: For the **GDC-0310** and compound **4** VSD4-Na_V1.7-
418 Na_VPas complexes, holey carbon grids (Ultrafoil 25 nM Au R 0.6/1 300 mesh; Quantifoil)
419 were incubated with a thiol reactive, self-assembling reaction mixture of 4mM
420 monothiolalkane(C11)PEG6-OH (11-mercaptoundecyl) hexaethyleneglycol (SPT-
421 0011P6, SensoPath Technologies, Inc., Bozeman, MT). Grids were incubated with this
422 self-assembled monolayer (SAM) solution for 24 hours and afterwards rinsed with EtOH.
423 3 µl of the sample was applied to the grid and blotted with Vitrobot Mark IV
424 (Thermofisher) using 3.5 s blotting time with 100% humidity and plunge-frozen in liquid
425 ethane cooled by liquid nitrogen. The **GNE-3565** VSD4-Na_V1.7-Na_VPas complex was,
426 similarly as described above, applied to a holey carbon grid (Ultrafoil 25 nM Au R 1.2/1,3
427 300 mesh; Quantifoil) pretreated with SAM solution. The grid was blotted single-sided
428 with a Leica EM GP (Leica) using 3 s blotting time with 100% humidity and plunge-frozen
429 in liquid ethane cooled by liquid nitrogen. For compound **2** VSD4-Na_V1.7-Na_VPas-DC1a
430 complex, holey carbon grids (Ultrafoil 25 nM Au R 2/2 200 mesh; Quantifoil) were glow-
431 discharged for 10 s using the Solarus plasma cleaner (Gatan). 3 µl of the sample was applied
432 to the grid and blotted with Vitrobot Mark IV (Thermofisher) using 2.5 s blotting time with
433 100% humidity and plunge-frozen in liquid ethane cooled by liquid nitrogen.
434
435 Movie stacks for compound **2** VSD4-Na_V1.7-Na_VPas-DC1a complex were collected using
436 SerialEM[48] on a Titan Krios operated at 300 keV with bioquantum energy filter equipped
437 with a K2 Summit direct electron detector camera (Gatan). Images were recorded at
438 165,000 × magnification corresponding to 0.824 Å per pixel, using a 20 eV energy slit.
439 Each image stack contains 50 frames recorded every 0.2 s for an accumulated dose of ∼50
440 e Å−2 and a total exposure time of 10 s. Images were recorded with a set defocus range of
441 0.5 to 1.5 µm.
442

443 Movie stacks for **GNE-3565, GDC-0310** and compound **4** VSD4-Na_V1.7-Na_VPas
444 complexes were collected using SerialEM on a Titan Krios G3i (ThermoFisher Scientific,
445 Waltham, MA) operated at 300 keV with bioquantum energy filter equipped with a K3
446 Summit direct electron detector camera (Gatan Inc, Pleasanton, CA). Images were recorded
447 in EFTEM mode at 105,000 × magnification corresponding to 0.838 Å per pixel, using a
448 20 eV energy slit. Each image stack contains 60 frames recorded every 0.05 s for an
449 accumulated dose of ∼60 e Å−2 and a total exposure time of 3 s. Images were recorded
450 with a set defocus range of 0.5 to 1.5 µm.
451
452 **CryoEM data processing**
453 CryoEM data were processed using a combination of the RELION[49] and cisTEM[50]
454 software packages, similarly as described previously[51] and as illustrated in Suppl. Figure 2
455 and 3.
456
457 Movies were corrected for frame motion using the MotionCor2[52] implementation in
458 RELION and contrast-transfer function parameters were fit using the 30-4.5 Å band of the
459 spectrum with CTFFIND-4.[53] CTF fitted images were filtered on the basis of the detected
460 fit resolution better than 6-10 Å. Particles were picked by template-matching with
461 gautomatch (https://www2.mrc-lmb.cam.ac.uk/research/locally-developed-
462 software/zhang-software/#gauto) using a 30 Å low-pass filtered apo VSD4-Na_V1.7-
463 Na_VPas reference structure. Particles were sorted during RELION 2D classification and
464 selected particles were imported into cisTEM for 3D refinements. 3D reconstructions were
465 obtained after auto-refine and manual refinements with a mask around the channel
466 (excluding the detergent micelle) and by applying low-pass filter outside the mask (filter
467 resolution 20 Å) and a score threshold of 0.10-0.30, so that only the best-scoring 10-30%
468 of particle images would be included in the 3D reconstruction at each cycle. The weight
469 outside of the mask was set to 0.8. No data beyond 3.0 Å for compound **4**, 3.4 Å for **GDC-**
470 **0310**, 3.7Å **GNE-3565** and 4.0 Å for compound **2** were used in the refinements. Phenix
471 ResolveCryoEM[54] density modification was applied to each of the reconstructions to
472 obtained the final map used for model building. Local resolution was determined in
473 cisTEM using a reimplementation of the blocres algorithm.
474
475 **Model building and structure analysis**
476 The previously determined VSD4-Na_V1.7-Na_VPas model (PDB: 6NT3)[21] was fit as a rigid
477 body into the cryoEM map. After manual adjustments, multiple rounds of real space
478 refinement using the phenix.real_space_refinement tool[55] was used to correct structural
479 differences between the initial model and the map. The small molecule coordinates were
480 generated with eLBOW,[56] placed and manually adjusted in Coot,[57] energy minimized with
481 MOE (Chemical Computing Group ULC,) and refined with real space refinements in
482 Phenix[55]. The model was validated using phenix.validation_cryoem[58] with built-in
483 MolProbity scoring.[59] Figures were made using PyMOL (The PyMOL Molecular Graphics
484 System, v.2.07 Schrödinger, LLC), UCSF Chimera,[60] and UCSF ChimeraX.[61]
485
486 **Chemical synthesis**

The synthesis of **GNE-3565**, **GDC-0310**, and compound **1** have been previously reported.[12,15,62] The synthesis and characterization of compounds **2-5** are described in the supporting information.

Na_V1.7 Syncropatch electrophysiology potency

cDNAs for Na_V1.7 (NM_002977) were stably expressed in Chinese Hamster Ovary (CHO) cells. Sodium currents were measured in the whole-cell configuration using Syncropatch 384PE (NanIon Technologies, Germany). 1NPC®-384 chips with custom medium resistance and single hole mode were used. Internal solution consisted of (in mM): 110 CsCl, 10 CsCl, 20 EGTA, and 10 Hepes (pH adjusted to 7.2); and external solution contains (in mM): 60 NMDG, 80 NaCl, 4 KCl, 1 $MgCl_2$, 2 $CaCl_2$, 2 D-Glucose monohydrate, 10 Hepes (pH adjusted to 7.4 with NaOH).

After system flushing, testing compounds were dissolved in external solution containing 0.1% Pluronic F-127. 10µl cells were added to the chip from a cell hotel, and a negative pressure of −50 mBar was applied to form a seal. Following treatment with seal enhancer solution and wash-off with external solution, negative pressure of −250 mbar was applied for 1 second to achieve the whole-cell configuration, followed by three washing steps in external solution. 20µl of compounds were added to 40µl in each well (1:3 dilution of compounds), and after mixing, 20µl was removed so the volume was retained at 40 ul. After approximately 13 minutes recording, 20µl/well of 2 uM TTX was added to achieve full block.

For voltage protocol, a holding potential of -50 mV was applied during the whole experiment. A depolarizing step was applied to -10mV for 10ms, followed by a hyperpolarization step to -150 mV for 20 ms to allow channel recovery from inactivation. A second depolarizing step was applied from -150mV to -10mV for 10 ms, where currents were measured to derive blocking effects of compounds. Inhibition was determined based on 7.5 min of compound incubation.

Figure Legends:

Figure 1: (A) Schematic of the VSD4-Na_V1.7-Na_VPas channel. The portions humanized to the Na_V1.7 sequence are shown in green. N-terminal domain (NTD) and CTD are indicated. **(B)** Side view of the single-particle cryo-EM reconstruction of VSD4- Na_V1.7-Na_VPas channel **(C-D)** Cartoon representations of the Top and Side views of VSD4-Na_V1.7-Na_VPas channel. Individual VSD domains are indicated. VSD4 is highlighted in green. **(E)** Localization of water molecules (in red) in the VSD4-Na_V1.7-Na_VPas channel structure. VSD4 is highlighted in green.

Figure 2: (A) Chemical structures of arylsulfonamide **GNE-3565**. **(B,C)** Top and Side views of VSD4-Na_V1.7-Na_VPas channel bound to **GNE-3565**. VSD4 is highlighted in green, **GNE-3565** in magenta. **(D)** Extracellular view of VSD4-Na_V1.7-Na_VPas arylsulfonamide receptor site is shown with select side chains rendered as sticks. **(E)** The cryoEM map surrounding the ligand **GNE-3565** is shown in mesh representation. **(F)** View towards the membrane highlighting key interactions with the **GNE-3565** warhead. **(G)**

View from the membrane highlighting key interactions with the **GNE-3565** central phenyl ring.

Figure 3: (A) Chemical structures of acylsulfonamide **GDC-0310**. **(B)** Top and Side views of VSD4-Na_V1.7-Na_VPas channel bound to **GDC-0310**. VSD4 is highlighted in green, **GDC-0310** in magenta. **(D)** Extracellular view of VSD4-Na_V1.7-Na_VPas acylsulfonamide receptor site is shown with select side chains rendered as sticks. **(E)** The cryoEM map surrounding the ligand **GDC-0310** is shown in mesh representation. **(F)** View towards the membrane highlighting key interactions with the **GDC-0310** warhead. **(G)** View from the membrane highlighting van der Waals interactions with the **GDC-0310** cyclopropyl substituent. The alpha-methylbenzylamine tail region sits almost entirely within the lipid bilayer.

Figure 4: (A) Illustration of hybrid molecule design approach. **(B)** Arylsulfonamide, acylsulfonamide and hybrid molecule poses **(C)** Hybridization strategy and molecule optimization. Highlighted are molecule **2** and molecule **4 (D)** Extracellular view of VSD4-Na_V1.7-Na_VPas bound to the hybrid molecule **2**. **(E)** View towards the membrane highlighting key interactions with the anionic group. **(F)** View from the membrane highlighting the lack of a stacking interaction between Y1537 and the phenyl ring. **(G)** Extracellular view of VSD4-Na_V1.7-Na_VPas bound to the hybrid molecule **4**. **(H)** View towards the membrane highlighting key interactions with the anionic group. **(I)** View from the membrane highlighting the π-stacking interaction between Y1537 and the phenyl ring.

Acknowledgments

We are grateful to BMR and RMG for construct generation and protein scale-up. We are thankful to Cameron Noland for help with the biochemistry of the VSD4-Na_V1.7-Na_VPas channel system. We thank Tommy Lai and Wenfeng Liu for chemistry support.

References

1. W. A. Catterall, A. L. Goldin, S. G. Waxman, International Union of Pharmacology. XLVII. Nomenclature and structure-function relationships of voltage-gated sodium channels. *Pharmacol. Rev.* **57**, 397 (2005).
2. C. A. Ahern, J. Payandeh, F. Bosmans, B. Chanda, The hitchhiker's guide to the voltage-gated sodium channel galaxy. *J. Gen. Physiol.* **147**, 1 (2016).
3. S. D. Dib-Hajj, Y. Yang, J. A. Black, S. G. Waxman, The Na(V)1.7 sodium channel: from molecule to man. *Nat. Rev. Neurosci.* **14**, 49 (2013).
4. J. Payandeh, D. H. Hackos, Selective ligands and drug discovery targeting the voltage-gated sodium channel Na_v1.7. *Handb. Exp. Pharmacol.* **246**, 271 (2018).
5. S. J. McKerrall, D. P. Sutherlin, Na_v1.7 inhibitors for the treatment of chronic pain. *Bioorg. Med. Chem. Lett.* **28**, 3141 (2018).
6. M. de Lera Ruiz, R. L. Kraus, Voltage-gated sodium channels: structure, function, pharmacology, and clinical indications. *J. Med. Chem.* **58**, 7093 (2015).

7. K. McCormack, *et al.*, Voltage sensor interaction site for selective small molecule inhibitors of voltage-gated sodium channels. *Proc. Natl. Acad. Sci. USA* **110**, E2724 (2013).
8. N. A. Swain, *et al.,* Discovery of clinical candidate 4-[2-(5-amino-1H-pyrazol-4-yl)-4-chlorophenoxy]-5-chloro-2-fluoro-N-1,3-thiazol-4-ylbenzenesulfonamide (PF-05089771): design and optimization of diaryl ether aryl sulfonamides as selective inhibitors of $Na_V1.7$. *J. Med. Chem.* **60**, 7029 (2017).
9. A. McDonnell, *et al.,* Efficacy of the $Na_V1.7$ blocker PF-05089771 in a randomised, placebo-controlled, double-blind clinical study in subjects with painful diabetic peripheral neuropathy. *Pain* **159**, 1465 (2018).
10. P. Siebenga, *et al.*, Lack of detection of the analgesic properties of PF-05089771, a selective $Na_V1.7$ inhibitor, using a battery of pain models in healthy subjects. *Clin. Transl. Sci.* **13**, 318 (2020).
11. M. E. Rothenberg, *et al.*, Safety, tolerability, and pharmacokinetics of GDC-0276, a novel $Na_V1.7$ inhibitor, in a first-in-human, single- and multiple-dose study in healthy volunteers. *Clin. Drug Investig.* **39**, 873 (2019).
12. B. S. Safina, *et al.*, Discovery of acyl-sulfonamide $Na_V1.7$ inhibitors GDC-0276 and GDC-0310. *J. Med. Chem.* **64**, 2953 (2021).
13. S. Noreng, T. Li, J. Payandeh, Structural pharmacology of voltage-gated sodium channels. *J. Mol. Bio.* **433**, 166967 (2021).
14. S. Ahuja, *et al.*, Structural basis of Nav1.7 inhibition by an isoform-selective small-molecule antagonist. *Science* **350**, aac5464 (2015).
15. S. Sun, *et al.*, Identification of selective acyl sulfonamide-cycloalkylether inhibitors of the voltage-gated sodium channel (Na_V)1.7 with potent analgesic activity. *J. Med. Chem.* **62**, 908 (2019).
16. M. Congreve, J. M. Dias, F. H. Marshall, Structure-based drug design for G protein-coupled receptors. *Prog. Med. Chem.* **53**, 1 (2014).
17. Y. Cheng, Membrane protein structural biology in the era of single particle cryo-EM. *Curr. Opin. Struct. Biol.* **52**, 58 (2018).
18. A. Balestrini, *et al.*, A TRPA1 inhibitor suppresses neurogenic inflammation and airway contraction for asthma treatment. *J. Exp. Med.* **218**, e20201637 (2021).
19. L. Rougé, *et al.*, Structure of CD20 in complex with the therapeutic monoclonal antibody rituximab. *Science* **367**, 1224 (2020).
20. H. Xu, *et al.*, Structural basis of $Na_V1.7$ inhibition by a gating-modifier spider toxin. *Cell* **176**, 702 (2019).
21. T. Clairfeuille, et al., Structural basis of α-scorpion toxin action on Na_V channels. *Science* **363**, eaav8537 (2019).
22. H. Shen, D. Liu, K. Wu, J. Lei, N. Yan, Structures of human Na_V 1.7 channel in complex with auxiliary subunits and animal toxins. *Science* **363**, 1303 (2019).
23. G. Huang, *et al.*, High-resolution structures of human $Na_V1.7$ reveal gating modulation through α-π helical transition of $S6_{IV}$. *Cell Rep.* **39**, 110735 (2022).
24. H. Shen, *et al.*, Structure of a eukaryotic voltage-gated sodium channel at near-atomic resolution. *Science* **355**, eaal4326 (2017).
25. H. Shen, *et al.*, Structural basis for the modulation of voltage-gated sodium channels by animal toxins. *Science* **362**, eaau2596 (2018).

26. M. Weiss, *et al.*, Sulfonamides as selective $Na_V1.7$ inhibitors: optimizing potency and pharmacokinetics while mitigating metabolic liabilities, *J. Med. Chem.* **60**, 5969 (2017).
27. R. F. Graceffa, *et al.*, Sulfonamides as selective $Na_V1.7$ inhibitors: optimizing potency, pharmacokinetics, and metabolic properties to obtain atropisomeric quinolinone (AM-0466) that affords robust in vivo activity, *J. Med. Chem.* **60**, 5990 (2017).
28. S. J. McKerrall, *et al.*, Structure- and ligand-based discovery of chromane arylsulfonamide $Na_V1.7$ inhibitors for the treatment of chronic pain, *J. Med. Chem.* **62**, 4091 (2019).
29. A. J. Roecker, *et al.*, Discovery of arylsulfonamide $Na_V1.7$ inhibitors: IVIVC, MPO methods, and optimization of selectivity profile, *ACS Med. Chem. Lett.* **12**, 1038 (2021).
30. T. Focken, *et al.*, Discovery of aryl sulfonamides as isoform-selective inhibitors of $Na_V1.7$ with efficacy in rodent pain models, *ACS Med. Chem. Lett.* **7**, 277 (2016)
31. Y-J. W., *et al.*, Development of new benzenesulfonamides as potent and selective $Na_V1.7$ inhibitors for the treatment of pain, *J. Med. Chem.* **60**, 2513 (2017).
32. J. Payandeh, M. Volgraf, Ligand binding at the protein-lipid interface: strategic considerations for drug design. *Nat. Rev. Drug Discov.* **20**, 710 (2021).
33. G. Bankar, et al., Selective $Na_V1.7$ antagonists with long residence time show improved efficacy against inflammatory and neuropathic pain. *Cell Rep.* **24**, 3133 (2018).
34. G. Luo, *et al.*, Discovery of indole- and indazole-acylsulfonamides as potent and selective $Na_V1.7$ inhibitors for the treatment of pain, *J. Med. Chem.* **62**, 831 (2019).
35. E. F. DiMauro, *et al.*, Application of a parallel synthetic strategy in the discovery of biaryl acyl sulfonamides as efficient and selective $Na_V1.7$ inhibitors, *J. Med. Chem.* **59**, 7818 (2016).
36. T. Focken, *et al.*, Design of conformationally constrained acyl sulfonamide isosteres: identification of N-([1,2,4]triazolo[4,3-a]pyridin-3-yl)methane-sulfonamides as potent and selective $hNa_V1.7$ inhibitors for the treatment of pain, *J. Med. Chem.* **61**, 4810 (2018).
37. X. Li, et al., Structural basis for modulation of human $Na_V1.3$ by clinical drug and selective antagonist. *Nat. Commun.* **13**, 1286 (2022).
38. N. K. Kotla, K. A. Kumari, S. K. Gunda, M. Shaik, 3D-QSAR and molecular docking studies of acylsulfonamides as $Na_V1.7$ inhibitors in chronic pain. *Res. J. Life Sci. Bioinform. Pharm. Chem. Sci.* **5**, 120 (2019).
39. R. P. Mason, D. G. Rhodes, L. G. Herbette, Reevaluating equilibrium and kinetic binding parameters for lipophilic drugs based on a structural model for drug interactions with biological membranes. *J. Med. Chem.* **34**, 869 (1991).
40. R. A. Coleman, M. Johnson, A. T. Nials, C. J. Vardey, Exosites: their current status, and their relevance to the duration of action of long- acting beta 2-adrenoceptor agonists. *Trends Pharmacol. Sci.* **17**, 324 (1996).
41. G. P. Anderson, A. Lindén, K. F. Rabe, Why are long-acting beta-adrenoceptor agonists long-acting? *Eur. Respir. J.* **7**, 569 (1994).
42. M. Masureel, *et al.*, Structural insights into binding specificity, efficacy and bias of a β2 AR partial agonist. *Nat. Chem. Biol.* **14**, 1059 (2018).

43. R. P. Austin, *et al*., QSAR and the rational design of long- acting dual D2-receptor/beta 2-adrenoceptor agonists. *J. Med. Chem*. **46**, 3210 (2003).
44. D. G. Rhodes, R. Newton, R. Butler, L. Herbette, Equilibrium and kinetic studies of the interactions of salmeterol with membrane bilayers. *Mol. Pharmacol.* **42**, 596 (1992).
45. D. A. Sykes, *et al.*, Observed drug- receptor association rates are governed by membrane affinity: the importance of establishing "micro- pharmacokinetic/ pharmacodynamic relationships" at the β2-adrenoceptor. *Mol. Pharmacol.* **85**, 608 (2014).
46. C. J. Dickson, *et al.*, Uncoupling the structure−activity relationships of β2 adrenergic receptor ligands from membrane binding. *J. Med. Chem.* **59**, 5780 (2016).
47. Z. Zhao, *et al.*, Exploration of type II binding mode: a privileged approach for kinase inhibitor focused drug discovery? *ACS Chem. Biol.* **9**, 1230 (2014).
48. D. N. Mastronarde, Automated electron microscope tomography using robust prediction of specimen movements. *J. Struct. Biol.* **152**, 36 (2005).
49. S. H. W. Scheres, RELION: implementation of a Bayesian approach to cryo-EM structure determination. *J. Struct. Biol.* **180**, 519 (2012).
50. T. Grant, A. Rohou, N. Grigorieff, *cis*TEM, user-friendly software for single-particle image processing. *Elife* **7**, e35383 (2018).
51. M. Kschonsak, *et al.* Structural architecture of the human NALCN channelosome. *Nature* **603**, 180 (2022).
52. S. Q. Zheng *et al.* MotionCor2: anisotropic correction of beam-induced motion for improved cryo-electron microscopy. *Nature Methods* **14**, 331 (2017).
53. A. Rohou, N. Grigorieff, CTFFIND4: Fast and accurate defocus estimation from electron micrographs. *J. Struct. Biol.* **192**, 216 (2015).
54. T. C. Terwilliger, S. J. Ludtke, R. J. Read, P. D. Adams, P. V. Afonine, Improvement of cryo-EM maps by density modification. *Nature Methods* **17**, 923 (2020).
55. P. V. Afonine, *et al*. Real-space refinement in PHENIX for cryo-EM and crystallography. *Acta Crystallogr. D. Struct. Biol.* **74**, 531 (2018).
56. N. W. Moriarty, R. W. Grosse-Kunstleve, P. D. Adams, electronic Ligand Builder and Optimization Workbench (eLBOW): a tool for ligand coordinate and restraint generation. *Acta Crystallogr. D. Biol. Crystallogr.* **65**, 1074 (2009).
57. P. Emsley, B. Lohkamp, W. G. Scott, K. Cowtan, Features and development of Coot. *Acta Crystallogr. D. Biol. Crystallogr.* **66**, 486 (2010).
58. P. V. Afonine, *et al*. New tools for the analysis and validation of cryo-EM maps and atomic models. *Acta Crystallogr. D Struct. Biol.* **74**, 814 (2018).
59. C. J. Williams, *et al*. MolProbity: More and better reference data for improved all-atom structure validation. *Protein Sci.* **27**, 293 (2018).
60. E. F. Pettersen, *et al*. UCSF Chimera--a visualization system for exploratory research and analysis. *J. Comput. Chem.* **25**, 1605 (2004).
61. T. D. Goddard, *et al.* UCSF ChimeraX: Meeting modern challenges in visualization and analysis. *Protein Sci.* **27**, 14 (2018).
62. D. Sutherlin *et al.* Therapeutic compounds and methods of use thereof. US11028075B2, June 8, 2021.

716
717
718
719

Figure 1

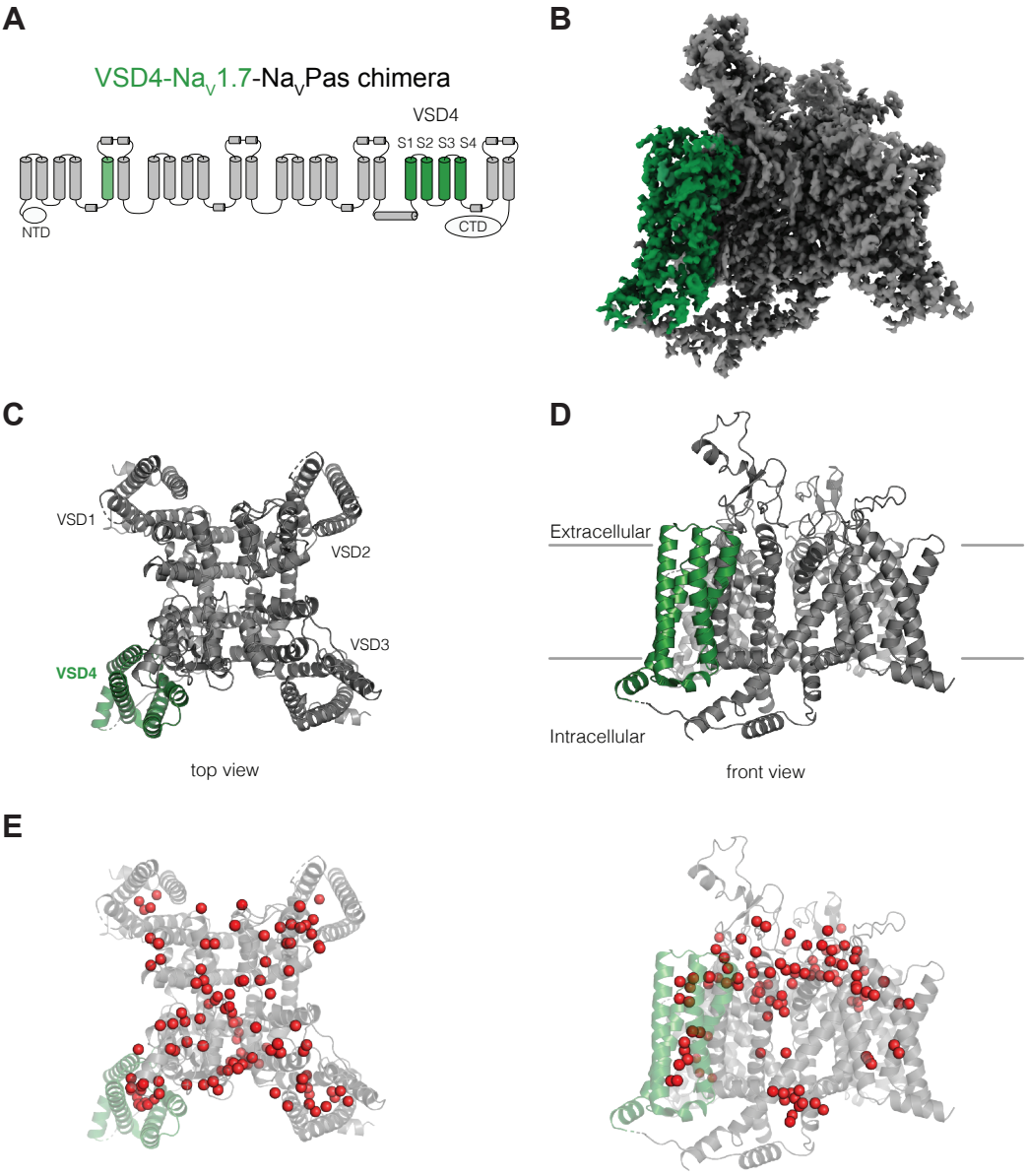
A
VSD4-Na$_V$1.7-Na$_V$Pas chimera
VSD4
S1 S2 S3 S4
NTD
CTD
B
C
VSD1
VSD2
VSD3
VSD4
top view
D
Extracellular
Intracellular
front view
E

Figure 2

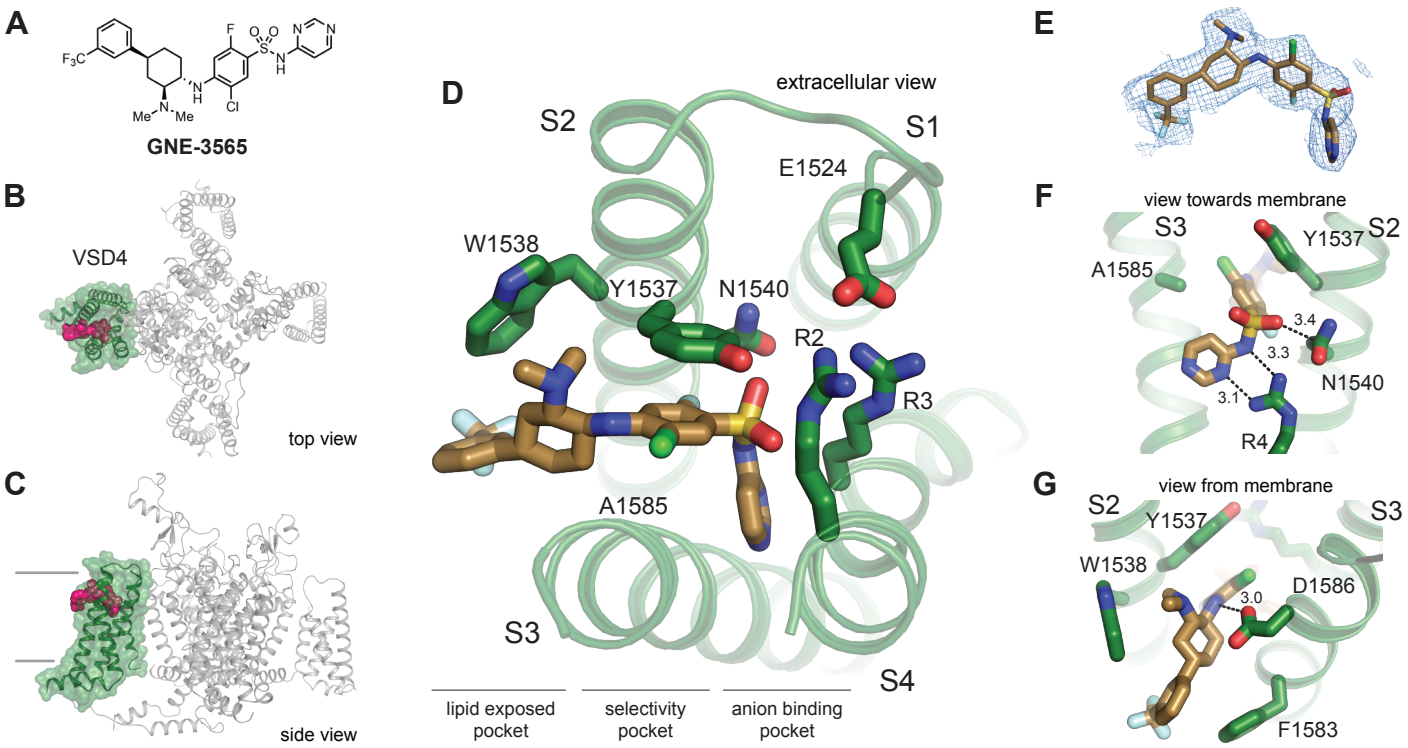
A
GNE-3565
B
VSD4
top view
C
side view
D
extracellular view
S2
S1
E1524
W1538
Y1537
N1540
R2
R3
A1585
S3
S4
lipid exposed pocket
selectivity pocket
anion binding pocket
E
F
view towards membrane
S3
S2
Y1537
A1585
3.4
3.3
3.1
N1540
R4
G
view from membrane
S2
Y1537
S3
W1538
D1586
3.0
F1583

Figure 3

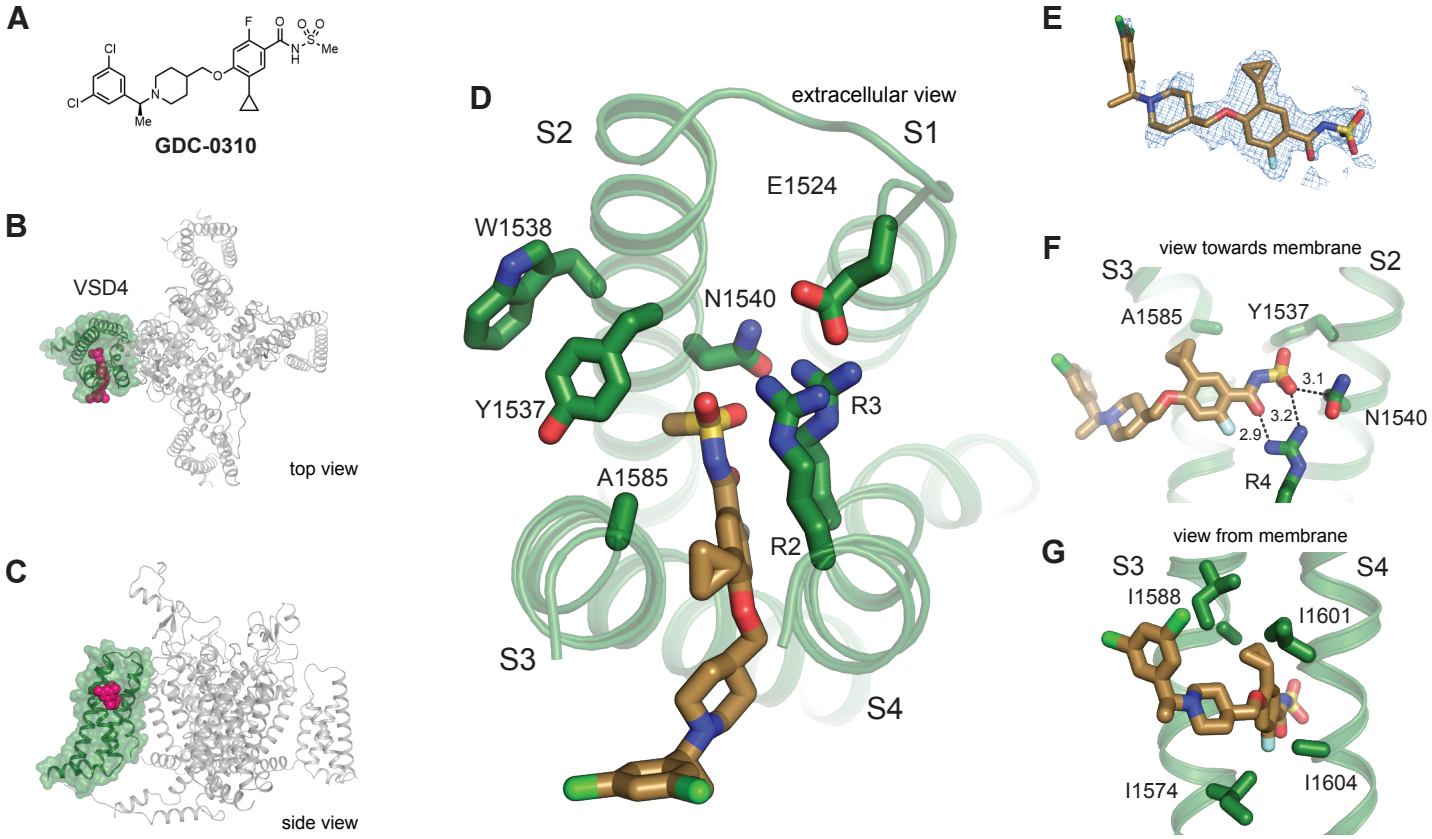
A
GDC-0310
B
VSD4
top view
C
side view
D
extracellular view
S2
S1
E1524
W1538
N1540
Y1537
R3
A1585
R2
S3
S4
E
F
view towards membrane
S3
S2
A1585
Y1537
3.1
3.2
2.9
N1540
R4
G
view from membrane
S3
S4
I1588
I1601
I1574
I1604

Figure 4

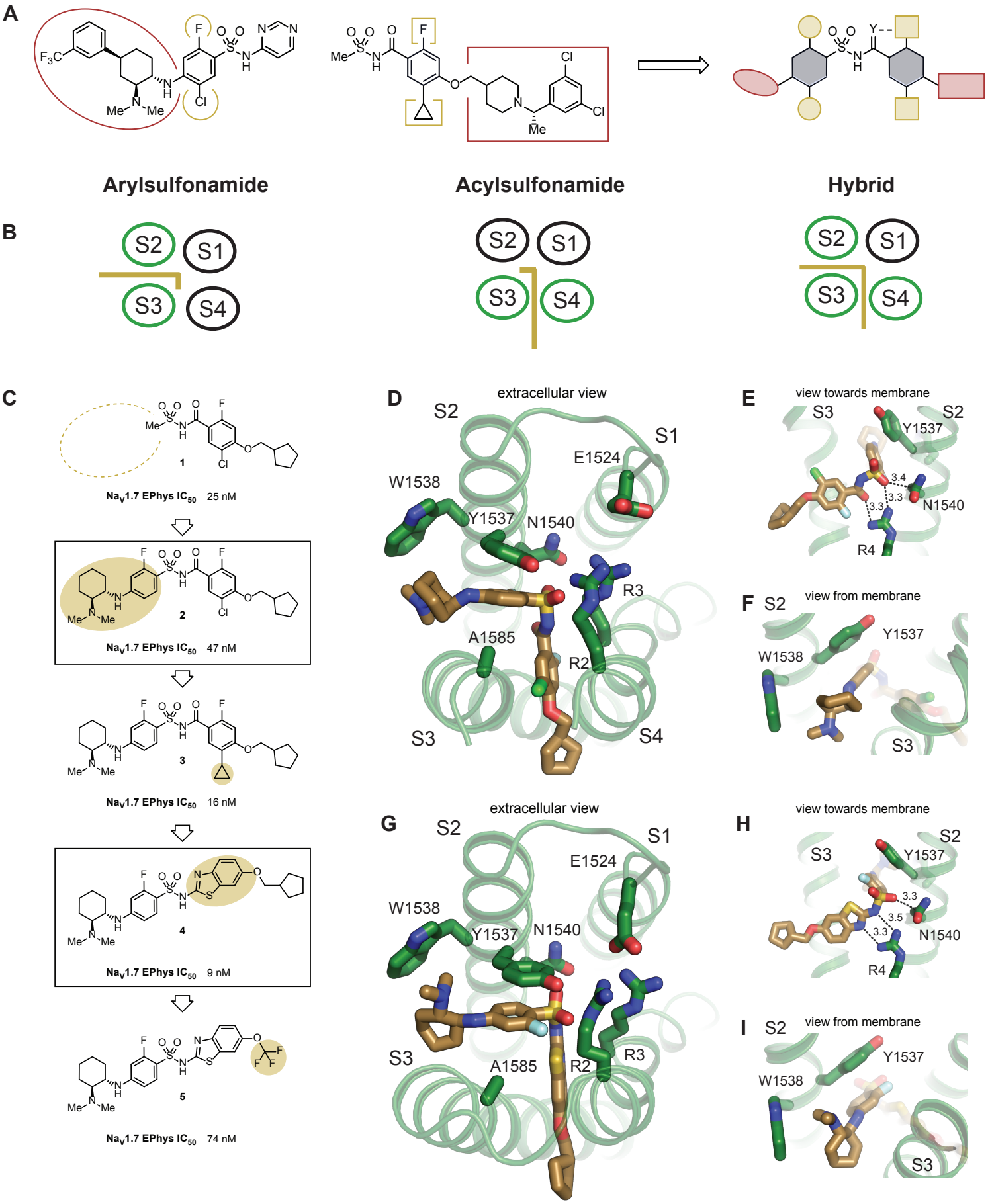
A
Arylsulfonamide
Acylsulfonamide
Hybrid
B
S2
S1
S3
S4
C
1
$Na_V1.7$ EPhys IC_{50} 25 nM
2
$Na_V1.7$ EPhys IC_{50} 47 nM
3
$Na_V1.7$ EPhys IC_{50} 16 nM
4
$Na_V1.7$ EPhys IC_{50} 9 nM
5
$Na_V1.7$ EPhys IC_{50} 74 nM
D
extracellular view
S2
S1
E1524
W1538
Y1537
N1540
R3
A1585
R2
S3
S4
E
view towards membrane
S3
S2
Y1537
3.4
3.3
3.3
N1540
R4
F
S2
view from membrane
Y1537
W1538
S3
G
extracellular view
S2
S1
E1524
W1538
Y1537
N1540
S3
A1585
R2
R3
H
view towards membrane
S3
S2
Y1537
3.3
3.5
3.3
N1540
R4
I
S2
view from membrane
Y1537
W1538
S3